

Thinning or thickening? Multiple rheological regimes in dense suspensions of soft particles

TAKESHI KAWASAKI, ATSUSHI IKEDA and LUDOVIC BERTHIER

Laboratoire Charles Coulomb, UMR 5221, CNRS and Université Montpellier 2, Montpellier, France

PACS 83.10.Mj – Molecular dynamics, Brownian dynamics
 PACS 83.80.Hj – Suspensions, dispersions, pastes, slurries, colloids
 PACS 83.80.Fg – Granular solids

Abstract. - The shear rheology of dense colloidal and granular suspensions is strongly nonlinear, as these materials exhibit shear-thinning and shear-thickening, depending on multiple physical parameters. We numerically study the rheology of a simple model of soft repulsive particles at large densities, and show that nonlinear flow curves reminiscent of experiments on real suspensions can be obtained. By using dimensional analysis and basic elements of kinetic theory, we rationalize these multiple rheological regimes and disentangle the relative impact of thermal fluctuations, glass and jamming transitions, inertia and particle softness on the flow curves. We characterize more specifically the shear-thickening regime and show that both particle softness and the emergence of a yield stress at the jamming transition compete with the inertial effects responsible for the observed thickening behaviour. This allows us to construct a dynamic state diagram, which can be used to analyze experiments.

Introduction. – Understanding the shear rheology of dense colloidal and granular suspensions remains a central challenge at the crossroad between nonequilibrium statistical mechanics and soft matter physics, with a clear technological relevance [1–3]. Simple liquids display simple rheological properties characterized by linear Newtonian behavior [4]. In a simple shear flow, for instance, the rate of deformation, $\dot{\gamma}$, is proportional to the applied shear stress, σ , such that the viscosity $\eta = \sigma/\dot{\gamma}$ uniquely characterizes the rheological response.

However, in dense particle suspensions such as emulsions, colloidal assemblies, or granular materials, the viscosity is usually not a single number, but a nonlinear function of the applied flow rate. To characterise these materials, an entire flow curve $\eta = \eta(\dot{\gamma})$ is thus needed [1–3]. Because the applied deformation now determines the response of the system, understanding nonlinear flow curves obviously requires a more detailed analysis, which must deal with both nonlinear and nonequilibrium effects. When the viscosity varies with the applied shear rate, the system can either flow more easily as $\dot{\gamma}$ increases (shear-thinning), or offer increasing resistance to flow (shear-thickening). We are familiar with both these effects, as most complex fluids used for cosmetics or in food products display these amusing nonlinearities, which

can be technologically both useful or annoying [3, 5].

In practice, most of experimental flow curves measured even in model suspensions display a complex mixture of both these nonlinear effects [2, 3, 5]. As two typical examples, we show flow curves measured in a colloidal dispersion of latex particles [5, 6] (diameter $a = 250$ nm, Fig. 1a), and in an oil-in-water emulsion [7] (diameter $a = 20$ μm , Fig. 1b). For a given volume fraction φ , the flow curves may display an initial Newtonian regime at low enough $\dot{\gamma}$ and φ , or a strong shear-thinning regime when φ is larger. This thinning regime is followed, for intermediate φ and larger $\dot{\gamma}$, by a Newtonian plateau regime. At larger $\dot{\gamma}$, shear-thickening sets in, and the magnitude of the viscosity increase clearly depends on the density regime. In some cases, shear-thickening is interrupted and flow curves display a viscosity maximum. Finally shear-thickening is not observed when density is too large, see for instance the large density data in Fig. 1b. Books and reviews of course offer an even broader range of possible behaviours [1–3, 5, 8, 9], but the data in Figs. 1a,b are representative of the typical behaviour of dense suspensions.

The primary purpose of this work is to show that a simple model of soft repulsive particles can exhibit a similarly complex rheology, despite the fact that *it does not incorporate* several of the physical ingredients usually put forward

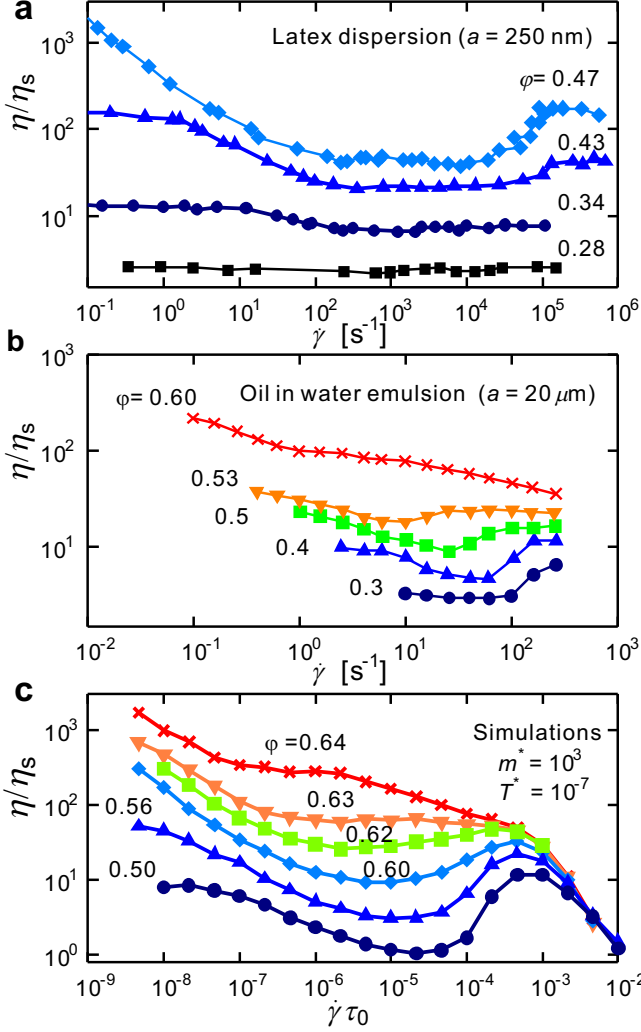


Fig. 1: Flow curves $\eta = \eta(\dot{\gamma})$ for various volume fractions ϕ obtained in two experimental systems (a,b) and measured in our numerical simulations (c). (a) Latex dispersion with diameter 250 nm [5,6]. (b) Oil-in-water emulsion with diameter 20 μm [7]. (c) Numerical simulations of harmonic spheres temperature and inertia included using adimensional parameters $T^* = 10^{-7}$ and $m^* = 10^3$. All three systems reveal a coexistence of multiple Newtonian, shear-thinning, and shear-thickening regimes, in a succession that strongly depends on volume fraction.

to account for these nonlinearities. We argue that understanding first such a simple model is useful before turning to more complicated physical explanations which can only increase the complexity of the results. In our model of spherical particles, we use a canonical pairwise, purely repulsive particle interaction. Dynamics is controlled by a traditional Langevin dynamics, which we simulate at either finite or zero temperature. The system is sheared at constant shear rate $\dot{\gamma}$ in a simple shear geometry, it flows homogeneously (no shear-banding) in the absence of any kind of density or stress gradients. We do not introduce more complex ingredients such as hydrodynamic interactions, attractive forces, lubrication forces, or fric-

tional contacts between the particles. Our model, we believe, represents an ideal starting point to understand the basic physics of suspensions, to which more ingredients could then be added, if needed.

In Fig. 1c, we present a set of flow curves obtained from our simulations, for a specific set of parameters, which we shall discuss shortly. For moderate volume fractions, we obtain a complex succession of Newtonian, shear-thinning, Newtonian, shear-thickening, shear-thinning regimes as the flow rate is varied. The first Newtonian regime disappears as ϕ is increased, and at even larger ϕ the intermediate Newtonian and thickening regimes also disappear, such that the flow curve becomes purely shear-thinning at large density. The existence of these multiple rheological regimes and their evolution with volume fraction is in excellent qualitative agreement with the experimental flow curves presented in Figs. 1a,b. Given the extreme simplicity of our model, we believe that such an agreement is an important achievement of our work.

In the following, we first summarize previous knowledge on nonlinear flow curves in dense suspensions. We then discuss our numerical results using dimensional analysis and basic elements of kinetic theory, and provide a simple understanding of all the regimes observed numerically.

Thinning and thickening. — Shear-thinning is the most commonly observed nonlinearity in experimental flow curves [1]. This effect typically results from the competition between the complex structure of the suspension under study that is responsible for the large viscosity of the system at rest, and the flow rate which tends to disrupt this static organization. For dense suspensions, large viscosities emerge when either the glass transition (for thermal systems [10]), or the jamming transition (for athermal ones [11]) is approached. In both cases, shear-thinning occurs when the shear rate competes with the relevant timescale associated to structural relaxation.

By contrast, shear-thickening is typically less common in experiments [8]. Additionally, its detailed characterization is more difficult, because shear-thickening is often mixed with issues such as flow heterogeneities, shear bands, density gradients, or particle migration [12,13]. However, shear-thickening has been documented for a large number of dense suspensions of various types, for soft and hard particles, for small colloids and large granular particles [3,5,8]. This variety of systems has led to a similar variety of theoretical arguments and models to account for shear-thickening, but a broad consensus has yet to emerge. In some systems, a strong increase of the viscosity can even become a nearly discontinuous jump, which we do not observe in our simple system. Another regime that we do not explore is suspensions at moderate densities, where a shear-thickening of modest amplitude likely results from hydrodynamic interactions promoting cluster formation under shear [5,14].

Recent experimental work conducted in dense suspensions shows that a shear-thickening of large ampli-

tude is observed in the vicinity of the jamming transition, suggesting that particle crowding promotes shear-thickening [9, 13, 15–23]. However, the emergence of a yield stress above the jamming transition was argued to suppress shear-thickening [9, 15], suggesting that some crowding is needed, but not *too much* crowding. These observations suggest that neglecting hydrodynamic interactions to focus instead on the specific competition between steric constraints and the shear flow is an interesting path.

Recent work [13, 18, 21] explored the idea that a strong continuous increase of the viscosity under shear results from a change of dissipation mechanism from viscous to inertial damping, in the spirit of Bagnold [24]. We extend these ideas to include also the effect of thermal fluctuations and particle softness, which are experimentally relevant. In recent work, we analysed in detail the complex interplay of thermal fluctuations and steric constraints in the overdamped limit [25, 26]. Here we add inertia, which introduces another timescale and adds a new level of complexity to flow curves that are already nontrivial.

For completeness, we mention recent studies invoking frictional forces to explain discontinuous shear-thickening [16, 17, 19–21, 23]. Numerical studies seem in good qualitative agreement with experiments, although quantitative understanding and detailed comparison to experimental data are unavailable.

Model and numerical simulations. – We study a system composed of N particles with equal mass m , interacting through a purely repulsive truncated harmonic potential [27], $V(r) = \frac{\epsilon}{2}(1 - r/a)^2\Theta(a - r)$, where a is particle diameter, ϵ an energy scale, and r the interparticle distance; $\Theta(x)$ is the Heaviside function. In practice, to avoid crystallization which might occur at large density, we use a 50 : 50 binary mixture of spheres with diameter ratio 1.4. The resulting volume fraction is $\varphi = \frac{\pi}{12L^3}N(a^3 + (1.4a)^3)$, where L is the linear size of the simulation box. We use $N = 10^3$ particles in a cubic box in three spatial dimensions, and enforce Lees-Edwards periodic boundary conditions [28].

These soft particles evolve with Langevin dynamics,

$$m \frac{d\vec{v}_i}{dt} + \xi(\vec{v}_i - \dot{\gamma} y_i \vec{e}_x) + \sum_{j \neq i} \frac{\partial V(|\vec{r}_i - \vec{r}_j|)}{\partial \vec{r}_i} + \vec{f}_i = 0, \quad (1)$$

where \vec{r}_i and \vec{v}_i respectively represent the position and velocity of particle i . The first term is the particle acceleration, and the second represents the viscous damping, controlled by the damping constant ξ . The system is sheared in the xy plane, and advection occurs along the x axis. The shear rate is $\dot{\gamma}$, y_i is the y coordinate of particle i , and \vec{e}_x is the unit vector along the x axis. The third term in Eq. (1) incorporates pairwise harmonic repulsion between the particles, and the final term is the Brownian random force acting on particle i , which we draw from a Gaussian distribution with zero mean and variance obeying the fluctuation-dissipation re-

lation, $\langle \vec{f}_i(t) \vec{f}_j(t')^T \rangle = 2k_B T \xi \delta_{ij} \mathbf{1} \delta(t - t')$, where k_B is the Boltzmann constant and T the temperature.

We impose the shear rate $\dot{\gamma}$ and measure the shear stress σ as the xy component of stress tensor using the Irving-Kirkwood formula [28]. We deduce the shear viscosity, $\eta = \sigma/\dot{\gamma}$.

Relevant timescales and units. – While very simple, Eq. (1) contains a number of distinct ingredients which typically control the physics of dense suspensions: inertial forces, viscous damping, particle interactions, and thermal noise. Their competition is more easily understood by introducing characteristic timescales to each term. We can define three independent timescales. The damping time of particle velocity is given by $\tau_v = m/\xi$. Energy is dissipated through viscous damping over a timescale $\tau_0 = \xi a^2/\epsilon$, while thermal fluctuations occur over a Brownian timescale $\tau_T = \xi a^2/(k_B T)$.

We can construct two dimensionless parameters out of these three timescales, which we will use to quantify the relative effects of inertia, thermal fluctuations and viscous damping. Comparing τ_v to τ_0 , we can create a dimensionless particle mass, $m^* = \tau_v/\tau_0 = m\epsilon/(\xi a)^2$. In the same spirit, comparing τ_T to τ_0 allows the definition of a dimensionless temperature, $T^* = \tau_T/\tau_0 = k_B T/\epsilon$. We use both T^* and m^* to specify the values of the control parameters employed in a given study, which amounts to choosing τ_0 as our microscopic time unit. Therefore a set of simulations is fully specified by the values of (m^*, T^*) , for which we can then vary both the packing fraction φ and the flow rate $\dot{\gamma}$.

We use the ‘solvent’ viscosity as a unit of viscosity, which is defined through the Stokes law, $\eta_s = \xi/(3\pi a)$. Accordingly, the natural stress scale is $\sigma_s = \epsilon/a^3$.

Multiple regimes in the flow curves. – Having defined the relevant timescales, we are now in a position to properly identify and interpret the multiple rheological regimes observed in the simulation results presented in Fig. 1c, which were obtained by fixing $m^* = 10^3$ and $T^* = 10^{-7}$. As should now be obvious, these values imply a clear separation of the relevant timescales, namely $\tau_T \gg \tau_v \gg \tau_0$. As a result, the imposed shear rate successively competes with all three timescales, which directly impacts the measured flow curves at various densities shown in Fig. 1c, as we now explain.

At $\varphi \leq 0.56$ a Newtonian behavior is observed in the limit $\dot{\gamma} \rightarrow 0$, which gives way to shear-thinning behaviour as $\dot{\gamma}$ is increased. Both these behaviours occur in the regime $\dot{\gamma}\tau_T \lesssim 1$, which implies that thermal fluctuations control this regime. ($\dot{\gamma}\tau_T$ is the ‘bare’ Péclet number). The corresponding Newtonian viscosity, η_T , is therefore directly related to the equilibrium structural relaxation timescale, $\tau_\alpha(T, \varphi)$, of the thermalized suspensions of harmonic spheres [29], which can be calculated through equilibrium linear response theory. Instead, shear-thinning is characteristic of the nonlinear rheology of viscous glassy fluids [10]. It occurs when structural relaxation is pro-

voked by the imposed shear flow (i.e. when the ‘dressed’ Péclet number $\dot{\gamma}\tau_\alpha$ is not small).

At higher shear rate, $\dot{\gamma}\tau_T \gtrsim 1$, thermal fluctuations cannot affect the physics which thus becomes equivalent to zero-temperature (or ‘athermal’) rheology [25]. In this regime, we first observe a Newtonian behavior, with an apparent viscosity η_0 which has a different value than in the first Newtonian regime, $\eta_0 \neq \eta_T$. The difference between these thermal and athermal Newtonian regimes for the overdamped case with $m^* = 0$ is discussed in Ref. [25]. Comparison with these earlier results reveals perfect agreement, which is expected as long as inertial effects do not affect the physics, i.e. when $\dot{\gamma}\tau_v$ is small.

Increasing further the shear rate, deviations from the overdamped limit start to appear when $\dot{\gamma}\tau_v$ becomes large [13, 18]. In this regime, we observe a succession of continuous shear-thickening followed by a shear-thinning regime. As a result, the viscosity exhibits a maximum at a well-defined $\dot{\gamma}$ value. The shear-thickening and the viscosity maximum are not present in the overdamped simulations [25], and are analysed in more detail below.

Having properly identified the various regimes, we turn to the evolution of the flow curves with volume fraction. The value of the viscosity η_T in the thermal Newtonian regime increases rapidly with φ as the glass transition density is approached, with $\varphi_g \approx 0.59$ [29], and the thermal regime is characterized by a strong shear-thinning behaviour, $\eta \propto \dot{\gamma}^{-1}$, as is typical for a glassy material with a finite yield stress.

The value of the second Newtonian viscosity η_0 in the athermal regime at larger $\dot{\gamma}$ also displays a strong increase with volume fraction, but with a density dependence distinct from the one of η_T , diverging near the jamming transition at $\varphi_J \approx 0.64$ [30].

An interesting behaviour is observed when the jamming transition is approached because η_0 increases more rapidly than the value of the viscosity maximum observed at the end of the shear-thickening regime. At a result, close enough to the jamming density these two values become equal, which implies that the shear-thickening regime eventually disappears as the volume fraction is larger than the jamming density, see Fig. 1c. Indeed, flow curves simplify above jamming and we simply observe shear-thinning behaviour for $\varphi \gtrsim 0.64$. In this density regime, the system behaves as a jammed athermal assembly of soft particles, and is therefore characterized by a finite yield stress [25, 30] which entirely dominates the flow curve, such that again $\eta \propto \dot{\gamma}^{-1}$.

A comparison to experimental flow curves in Figs. 1a,b shows that all features described in the simulations are also present in experiments. The thermal Newtonian and shear-thinning regimes, and the glass transition physics are observed in the colloidal latex dispersion at small shear rates (small Péclet number). The athermal Newtonian viscosity is observed in both the colloidal dispersion at large enough $\dot{\gamma}$ (large Péclet number), and in the emulsion where the large droplet size ensures that thermal fluctuations

are irrelevant. The strong continuous shear-thickening is also observed in both systems at larger shear rates, with a viscosity maximum also observed in some cases. Finally, when the soft emulsion is compressed above jamming, shear-thickening is not observed anymore. All these features are in excellent agreement with our numerical observations, as claimed in the introduction.

Scaling analysis of shear thickening. – We now focus on the specific deviations brought about by the inclusion of inertia into the equation of motion Eq. (1). To simplify the discussion, it is useful to analyse the case where thermal fluctuations are completely absent, $T^* = 0$, such that the competition is between viscous dissipation, inertial effects, and particle softness in the vicinity of the jamming transition. In other words, we consider the physics at large Péclet number.

We first concentrate on a fixed volume fraction below the jamming transition, $\varphi = 0.6 < \varphi_J$, and study the evolution of the flow curves as m^* is varied over a broad range, see Fig. 2a. For the smaller value, $m^* = 10$, inertia has a negligible effect on the flow curves, which thus resemble the result obtained in the overdamped limit $m^* = 0$, namely a Newtonian plateau with viscosity η_0 , followed by shear-thinning at large $\dot{\gamma}$. When m^* is increased, inertial effects set in and the shear-thickening behaviour and viscosity maximum become apparent. Clearly, the onset of shear-thickening, the magnitude of the viscosity increase, and the viscosity maximum are strongly dependent on m^* , showing that they directly result from inertial effects.

In Fig. 2b, we show the same data using a rescaled shear rate $\dot{\gamma}\tau_v$, using the inertial timescale $\tau_v = m/\xi$ defined above. Because τ_v is the typical relaxation time of particle velocities due to the viscous damping, the condition $\dot{\gamma}\tau_v \gg 1$ means that shear deformation occurs faster than velocity relaxation. In this rescaled plot, the onset of shear-thickening in the flow curves at various m^* collapses very nicely, such that $\eta \approx \eta_0$ when $\dot{\gamma}\tau_v \lesssim 10^{-2}$, while the data suggest $\eta \propto \dot{\gamma}^2$ when $\dot{\gamma}\tau_v \gtrsim 10^{-2}$. While the scaling variable $\dot{\gamma}\tau_v$ is a straightforward choice (justified below), the very small value it takes at the crossover, $\dot{\gamma}\tau_v \approx 10^{-2}$, is less intuitive.

We now rationalize the observed behaviours by developing theoretical arguments in the spirit of kinetic theory. The sole source of dissipation in the Langevin dynamics Eq. (1) is the viscous damping. Energy balance between dissipation and energy injection by the flow per unit volume and unit time yields

$$\sigma\dot{\gamma} = \rho L^3 \times \xi \bar{v}^2 / L^3, \quad (2)$$

where \bar{v} is the typical amplitude of the particle velocity. Using a kinetic theory argument, the shear stress can also be expressed as the product of a number of collisions with a typical momentum transfer at collisions. Neglecting the density dependence of the mean free path, this gives us a second (approximate) relation:

$$\sigma \approx \rho L^2 \bar{v} \times m \dot{\gamma} a / L^2. \quad (3)$$

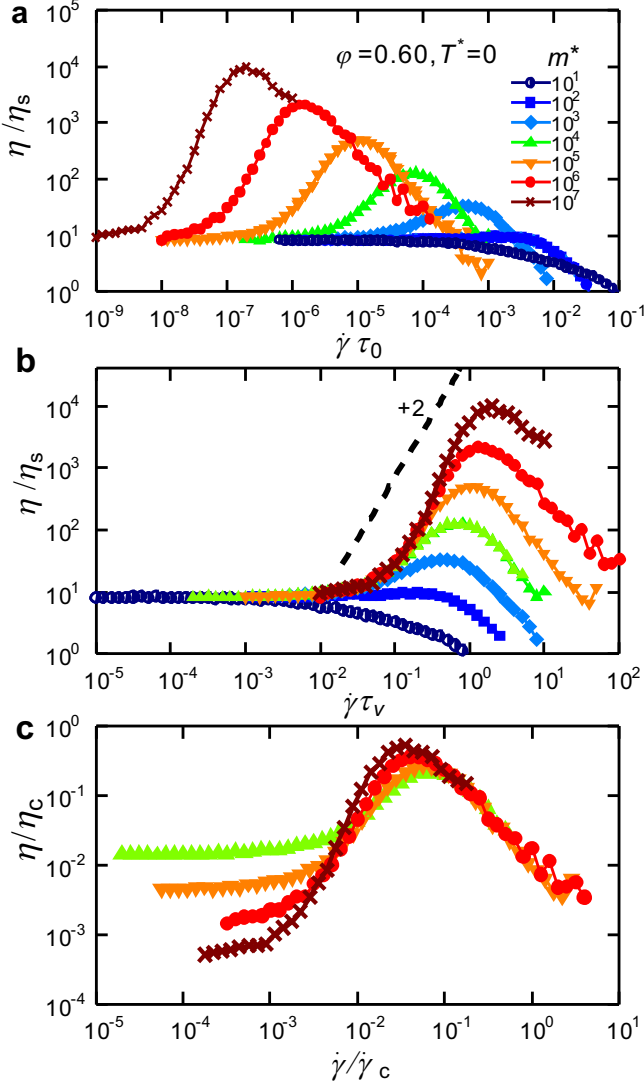


Fig. 2: Flow curves obtained zero temperature, $T^* = 0$, and $\varphi = 0.6$ for increasing mass m^* . (a) Raw viscosity data indicate the emergence of shear-thickening with onset and magnitude controlled by inertial terms. (b) Same data plotted as a function of the rescaled flow rate $\dot{\gamma}\tau_v$ display a good collapse of the onset of shear-thickening near $\dot{\gamma}\tau_v \approx 10^{-2}$, followed by a regime with $\eta \propto \dot{\gamma}^2$, see Eq. (4). (c) Scaling plot of the viscosity maximum with parameters taken from Eq. (5).

By combining Eqs. (2, 3) we obtain:

$$\sigma \approx (\rho m^2 a^2 / \xi) \dot{\gamma}^3, \quad \bar{v} \approx (ma / \xi) \dot{\gamma}^2. \quad (4)$$

Remarkably, the obtained constitutive equation between stress and shear rate fully agrees with the observation $\eta/\eta_s \propto (\tau_v \dot{\gamma})^2$ in Fig. 2b. Note that this result is different from Bagnold scaling $\eta \propto \dot{\gamma}$ [24], because the shear rheology in this regime strongly depends on the details of the energy dissipation [31]. Bagnold scaling is obtained when energy dissipation in Eq. (1) is introduced via collisions, such that the energy balance equation in Eq. (2) is modified into $\sigma \dot{\gamma} \propto \bar{v}^3$. Together with Eq. (3), Bagnold scaling $\eta \propto \bar{v}^2$ would be recovered [32].

We can extend our kinetic argument to account for the effect of particle softness and explain the origin of the viscosity maximum. The above analysis suggests that particles move faster as $\dot{\gamma}$ increases, see Eq. (4). This implies that ‘collisions’ become ill-defined when particles have enough kinetic energy to overcome their repulsive interactions, which happens when $\bar{v} > \bar{v}_c$ with the crossover velocity \bar{v}_c given by: $m\bar{v}_c^2/2 \approx \epsilon$. Combined with Eq. (4) this argument provides a rough estimate of the height and location of the viscosity maximum, namely

$$\eta_c = \rho a (m\epsilon)^{1/2}, \quad \dot{\gamma}_c = [\epsilon \xi^2 / (m^3 a^2)]^{1/4}. \quad (5)$$

In Fig. 2c, the renormalized flow curves η/η_c versus $\dot{\gamma}/\dot{\gamma}_c$ are shown, where the height and location of the viscosity maxima are nearly collapsed, suggesting that our crude argument captures its origin, namely, the competition between inertial effects and particle softness. For collisional dissipation and soft particles, we predict again a viscosity maximum [33] but with different scaling properties controlled by $\eta_c = \rho a (m\epsilon)^{1/2}$ and $\dot{\gamma}_c = [\epsilon / (ma^2)]^{1/2}$.

Dynamic state diagram. — So far, we analysed the shear-thickening at constant density. To obtain a dynamic state diagram of the multiple rheological regimes as determined experimentally [15], we turn to the influence of the volume fraction. We concentrate again on the zero-temperature case, for convenience. In Fig. 3a, we show flow curves with $T^* = 0$, $m^* = 10^5$, and various volume fraction from $\varphi = 0.58$ below jamming up to $\varphi = 0.66$ above, while Fig. 3b summarizes these results in a stress / volume fraction dynamic state diagram [15].

The data in Fig. 3a suggest that the onset of shear-thickening is only very weakly dependent on the volume fraction, and occurs when $\dot{\gamma}\tau_v \approx 10^{-2}$ independently of φ . (We have validated this hypothesis for a much broader range of control parameters [33].) This indicates that the volume fraction dependences of the Newtonian viscosity η_0 and of the inertial regime $\eta \propto \dot{\gamma}^2$ are actually identical, suggesting that both regimes actually reflect the fundamental flow properties of an athermal assembly of hard spherical particles below jamming. Accordingly, the stress scale controlling the Newtonian-to-thickening transition in Fig. 3b is given by $\sigma \approx \eta_0(\varphi) \times 10^{-2} / \tau_v$, and its evolution with φ is thus essentially controlled by the one of the viscosity $\eta_0(\varphi)$, which diverges at φ_J . Our simulations also indicate that the density dependence of the stress maximum is nonsingular, see Fig. 3a. The stress scale delimiting the upper boundary of the shear-thickening region in Fig. 3b is thus nearly constant.

When the jamming transition is approached, both Newtonian and shear-thickening regimes disappear. The former because it becomes easier to enter the shear-thinning regime as the viscosity η_0 increases [30]. The latter regime disappears when the viscosity in the Newtonian plateau becomes larger than the viscosity maximum at the end of the thickening regime, which happens at a density slightly below jamming. These two stress boundaries are reported

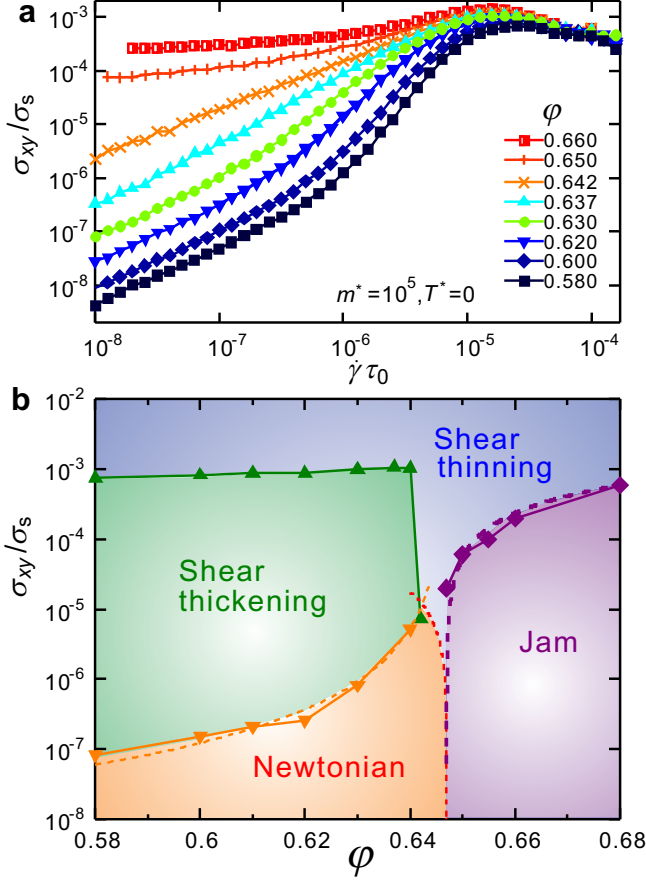


Fig. 3: (a) Evolution with volume fraction of the flow curves obtained for $T^* = 0$ and $m^* = 10^5$. (b) Dynamic state diagram for the same parameters showing stress regions where Newtonian, shear-thickening and shear-thinning regimes can be observed. The system does not flow in the ‘jam’ region, where the stress is below the yield stress value.

in the diagram of Fig. 3b, which shows that the jammed system at $\phi > \phi_J$ either does not flow when σ is below the yield stress (which increases continuously with density above ϕ_J [25]), or displays shear-thinning. The overall structure of the state diagram is similar to the experimental results [15].

We have shown that a simple Langevin model of soft repulsive particles displays a rheology in good agreement with the complex rheology observed in dense suspensions, due to the timescale competition between τ_0 , τ_T and τ_v . Our simulations indicate in particular that the onset of shear-thickening occurs when $\dot{\gamma}\tau_v \approx 10^{-2}$, which agrees excellently with the value $\dot{\gamma}\tau_v \sim 0.7 \cdot 10^{-2}$ obtained in Fig. 1b for the emulsion, while a somewhat smaller value $\dot{\gamma}\tau_v \sim 0.4 \cdot 10^{-3}$ is found for the latex dispersion shown in Fig. 1a. We note that the addition of frictional forces might affect the nature of the shear-thickening onset [19, 20], but not necessarily the shear rate where it occurs [21].

REFERENCES

- [1] R. G. Larson, *The Structure and Rheology of Complex Fluids* (Oxford University Press, New York, 1999).
- [2] P. Coussot, *Rheometry of Pastes, Suspensions, and Granular Materials* (Wiley, New York, 2005).
- [3] J. M. Norman and N. J. Wagner, *Colloidal Suspension Rheology* (Cambridge University Press, 2012).
- [4] J. P. Hansen and I. R. McDonald, *Theory of Simple Liquids*, (Elsevier, Amsterdam, 1986).
- [5] N. J. Wagner and J. F. Brady, *Phys. Today* **62**, No. 10, 27 (2009).
- [6] H. M. Laun, *Angew. Makromol. Chem.* **123**, 335 (1984).
- [7] Y. Otsubo and R. K. Prud’homme, *Rheol. Acta* **33**, 29 (1994).
- [8] H. A. Barnes, *J. Rheol.* **33**, 329 (1989).
- [9] E. Brown and H. Jaeger, *Rep. Prog. Phys.* **77** 046602 (2014).
- [10] L. Berthier and G. Biroli, *Rev. Mod. Phys.* **83**, 587 (2011).
- [11] A. J. Liu, M. Wyart, W. van Saarloos and S. R. Nagel in *Dynamical heterogeneities in glasses, colloids and granular materials*, Eds.: L. Berthier, G. Biroli, J.-P. Bouchaud, L. Cipelletti, and W. van Saarloos, (Oxford University Press, Oxford, 2011).
- [12] A. Fall, N. Huang, F. Bertrand, G. Ovarlez, and D. Bonn, *Phys. Rev. Lett.* **100** 018301 (2008).
- [13] A. Fall, A. Lemaître, F. Bertrand, D. Bonn, and G. Ovarlez, *Phys. Rev. Lett.* **105**, 268303 (2010).
- [14] J. F. Brady and G. Bossis, *J. Fluid Mech.* **155**, 105 (1985).
- [15] E. Brown and H. M. Jaeger, *Phys. Rev. Lett.* **103**, 086001 (2009).
- [16] E. Brown and H. M. Jaeger, *J. Rheol.* **56**, 875 (2012).
- [17] M. Otsuki and H. Hayakawa, *Phys. Rev. E* **83**, 051301 (2011).
- [18] M. Trulsson, B. Andreotti, and P. Claudin, *Phys. Rev. Lett.* **109**, 118305 (2012).
- [19] R. Seto, R. Mari, J. F. Morris, and M. M. Denn, *Phys. Rev. Lett.* **111**, 218301 (2013).
- [20] R. Mari, R. Seto, J. F. Morris, and M. M. Denn, *arXiv:1403.6793*.
- [21] N. Fernandez, R. Mani, D. Rinaldi, D. Kadau, M. Mosquet, H. Lombois-Burger, J. Cayer-Barrioz, H. J. Herrmann, N. D. Spencer, and L. Isa, *Phys. Rev. Lett.* **111**, 108301 (2013).
- [22] W. Zheng, Y. Shi, N. Xu, *arXiv:1304.4993*.
- [23] C. Heussinger, *Phys. Rev. E* **88**, 050201 (2013).
- [24] R. A. Bagnold, *Proc. R. Soc. A* **225**, 49 (1954).
- [25] A. Ikeda, L. Berthier, and P. Sollich, *Phys. Rev. Lett.* **109**, 018301 (2012).
- [26] A. Ikeda, L. Berthier, and P. Sollich, *Soft Matter* **9**, 7669 (2013).
- [27] D. J. Durian, *Phys. Rev. Lett.* **75**, 4780 (1995).
- [28] M. Allen and D. Tildesley, *Computer Simulation of Liquids* (Oxford University, New York, 1987).
- [29] L. Berthier and T. A. Witten, *EPL* **86**, 10001 (2009).
- [30] P. Olsson and S. Teitel, *Phys. Rev. Lett.* **99**, 178001 (2007).
- [31] D. Vagberg, P. Olsson, and S. Teitel, *arXiv:1311.4902*.
- [32] N. Mitarai and H. Nakanishi, *Phys. Rev. Lett.* **94**, 128001 (2005).
- [33] T. Kawasaki, A. Ikeda, and L. Berthier, in preparation.